Purdue University
Purdue e-Pubs

CTRC Research Publications | Cooling Technologies Research Center

2014

Investigation of Boiling Heat Transfer in Water using a Free-Particles-Based Enhancement Technique

T. Y. Kim

Follow this and additional works at: http://docs.lib.purdue.edu/coolingpubs

Kim, T. Y., "Investigation of Boiling Heat Transfer in Water using a Free-Particles-Based Enhancement Technique" (2014). *CTRC Research Publications.* Paper 223.
http://dx.doi.org/http://dx.doi.org/10.1016/j.ijheatmasstransfer.2013.12.071

This document has been made available through Purdue e-Pubs, a service of the Purdue University Libraries. Please contact epubs@purdue.edu for additional information.

Investigation of boiling heat transfer in water using a free-particles-based enhancement technique

Tae Young Kim[a] and Suresh V. Garimella[b,†]

[a]Engine Research Lab
Korea Institute of Machinery & Materials
Daejeon 305-343, Republic of Korea

[b]Cooling Technologies Research Center, an NSF IUCRC
School of Mechanical Engineering, Purdue University
585 Purdue Mall, West Lafayette, IN 47907-2088 USA

Abstract

Enhancement of pool boiling heat transfer in water by means of the introduction of free particles on the heated surface is investigated. The layer of loose particles on the heated surface is free to move and deform under the action of bulk liquid convection and vapor nucleation. High-speed visualizations show that bubble nucleation preferentially occurs at the narrow corner cavities formed between the free particles and the heated surface. The effects of the number and size of the free particles are experimentally explored using copper particles over a wide size range from tens of nanometers to 13 mm. Experimental results show that a mixture of free particle diameters of 3 mm and 6 mm provides the greatest improvement in boiling heat transfer, resulting in an average increase in heat transfer coefficient of 115% relative to a baseline polished surface without particles. A numerical heat transfer simulation and an analytical force balance model are developed to predict nucleation incipience and explain the parametric trends in boiling performance observed in the presence of the free particles.

Keywords: Phase change, free particles, pool boiling enhancement, nucleation, water

† Corresponding author, Phone: 765-494-5621, sureshg@purdue.edu

Nomenclature

A	area
F	force
h	height, heat transfer coefficient
q	heat flux
r	radius
R	particle radius in y-direction
R_{RMS}	root-mean-squared surface roughness
ΔT	wall superheat
x	x-direction
y	y-direction

Greek

ρ	density
σ	surface tension
θ	solid-liquid-vapor contact angle
Ψ	sphericity

Subscripts

b	bubble, buoyancy force, liquid-vapor-particle contact point
c	liquid-vapor-particle contact point, capillary force
cb	capillary force at liquid-vapor-surface contact point
ct	capillary force at liquid-vapor-particle contact point
dep	departure
e	effective force
f	point of force
l	liquid
p	particle
w	water

1. Introduction

The heat dissipation efficiency of phase-change processes for cooling high-performance microprocessors, and thermal management of industrial engines, reactors, and plants, has motivated development of numerous techniques for pool boiling heat transfer enhancement. As the performance and density of modern electronics and elecromechanical systems rapidly increases, and phase-change

cooling becomes more prevalent, concepts for facilitating bubble nucleation at reduced superheat temperatures and intensifying the nucleate boiling process have been widely explored for heat transfer enhancement. As summarized by Webb [1], boiling heat transfer enhancement techniques usually fall into three categories: integral surface roughness, surface coatings, and attached nucleation promoters.

While surface roughening is well known to provide improvement in boiling heat transfer [2-5], reliance on this enhancement approach has generally been commercially intractable due to aging effects and difficulty in achieving repeatable and predictable performance. Jakob [6], Corty and Foust [7], and Chaudhri and McDougall [8] all investigated long-term reliability of roughened surfaces and found only temporary benefits from the treatment on boiling enhancement; the performance reverted to the level of the untreated surfaces within several hours. As an alternative, since the contact angle of a liquid on a heated surface affects bubble nucleation, nonwetting surface coatings such as paraffin and Teflon have been investigated [9-11]. Since nonwetting coatings provide nucleation sites at a lowered surface superheat compared to wetting surfaces, nucleate boiling heat transfer is improved at low heat fluxes; however, the large contact angle limits nucleation site density and vapor blanketing of the surface occurs at a lowered superheat. Nonwetting coatings of low thermal conductivity can also increase the surface thermal resistance. Patterning of a surface with alternating wetting and nonwetting areas to circumvent this challenge inherent to homogeneous non-wetting coatings was recently proposed [12].

Significant enhancement of pool boiling has been realized using various types of attached promoters, such as porous particle layers [13-18], wire meshes [19], and pin-fin structures [20,21]. These promoters are usually thermally conductive and directly attached to the heated surface. Compared to smooth surfaces, changes in local surface topography due to the presence of the attached promoters facilitates bubble nucleation at lower wall superheats, and results in more effective heat transfer from the surface to the working fluid. In order to improve both the nucleate boiling heat transfer coefficient and increase critical heat flux (CHF), the microscale structures in these studies were also designed to reduce liquid-vapor counterflow resistance. Despite the nucleate boiling heat transfer improvement achieved, the cumbersome processes required for fabrication of these microstructures on a boiling surface was often considered a drawback. Therefore, simpler methods were proposed for spraying/painting a mixture of metal particles, binder, and carrier on a target surface to form particulate porous layers [22,23]; however, deterioration of boiling heat transfer was reported as a result of the increase in thermal resistance between the heated surface, particles, and working fluid due to the thermally nonconductive binder used.

An additional enhancement technique not captured above is through the use of fluid additives. In particular, use of nanoscale particles as additives in nanofluids for boiling heat transfer enhancement has been widely studied, but the results have been inconclusive at best. A range of observations, such as mild

improvement [24,25], mild deterioration [26], and negligible impact [27] on boiling heat transfer, have been reported for nanofluids. A common observation, however, was the improvement in CHF reported in several studies [28,29] and primarily attributed to a deposition of thin particle layers on the heated surface during the nucleate boiling process. The deposited particle layers increased surface wettability, leading to a decrease in the contact angle between the surface and the working fluid, and thus in an enhancement of CHF. In a related approach, the concept of a free-particle technique for boiling heat transfer enhancement was proposed in the companion paper by Kim *et al*. [30] and experimentally investigated using the wetting fluid FC-72 as the working fluid. This technique introduces free-standing metal particles, which may be orders of magnitude larger than nanoparticles, on an immersed boiling surface. The primary function of the particles is to change the local surface topography by forming narrow corner gaps between the particle and the surface; these cavities promote bubble nucleation, and consequently enhance nucleate boiling at low heat fluxes. This nucleation enhancement mechanism is similar to conventional porous-structure attached promoters, except that the particles are not affixed to the heated surface and are free to move. Li and Cheng [31] described heterogeneous bubble nucleation density using classical kinetics of nucleation [32,33]. Due to the presence of the corner geometry, the incipient superheat is decreased compared to a flat surface. As reported in the literature [13,15,18,34-37], a decrease in the incipient wall superheat for surfaces coated with sintered particle layers is attributed to corner cavities formed where the particles attach to the heated surface. Similarly, in the free-particle technique, narrow corner gaps formed between the particles and the heated surface preferentially serve as active nucleation sites, and as a result, the wall superheat needed for boiling incipience decreases.

The influence of free particle size and number was investigated for FC-72 in a related study [30]. Since bubble nucleation and the onset of nucleate boiling (ONB) depend strongly on the properties of the working fluid [3, 38-41], the present study investigates the effect of the introduction of free copper particles on boiling of water, which has drastically different thermophysical properties compared to FC-72. The experiments show a particle size range of 3 mm to 6 mm is optimum for water with its high surface tension. Significantly smaller microscale particles were identified as an optimum for the low surface tension liquid, FC-72 [30].

2. Experimental setup and procedures

A schematic diagram of the pool boiling facility used for in current study is presented in Fig. 1. A detailed description of the facility, test procedures, and data reduction method is available in the companion study in [30], and a summary is provided here.

An insulated copper heating block forms the base of a sealed liquid bath test chamber. The polished (R_{RMS} = 25 nm, NewView 6200, Zygo Corp.) top 25.4 mm × 25.4 mm test surface of the heating block is exposed to the working fluid. A uniform heat flux is supplied to the test surface through 12 cartridge heaters embedded in the copper block; the block temperature is monitored by a rake of embedded T-type thermocouples. The side and bottom surfaces of the copper are shrouded by ceramic insulation and installed into a PEEK housing. To seal the test surface into this heater assembly, sealant and epoxy layers are applied around the edge of the test surface of the heating block, as shown in Fig. 1. This assembly is attached to the bottom of the square polycarbonate liquid tank. A stainless steel condenser coil (not shown in Fig. 1) with a circulating 50-50 water-glycol mixture at 44 °C condenses vaporized working fluid. The tank is connected to an ice bath vapor trap open to the ambient, which ensures that all tests are performed at atmospheric pressure.

To perform a test, the tank is filled with 45 ml of water, and the water is boiled for two hours using a cartridge heater inserted through the top housing and the cartridge heaters embedded in the copper heating block to degas the fluid and test surface. After the degassing process, 20 ml of the working fluid is quickly drained using a syringe while the fluid in the test section remains at the saturation temperature (to prevent uptake of air) so that 25 ml of fluid remains in the test section. The desired quantity of copper free particles of specified size are gently placed on the heated surface. The heater block and pool temperatures are continuously monitored with a data acquisition system. To measure the performance for each set of free particles, the power input is incremented through different heat flux levels. The maximum heat flux is limited to 100 kW/cm^2 because vigorous boiling at this heat flux causes the liquid bath to come in direct contact with the condenser coil; therefore, CHF measurements are not acquired when using water as the working fluid. (In companion experiments with FC-72 [30], the tests were run to CHF at 160 kW/cm^2; the smaller departing vapor bubbles due to the lower surface tension in that case mitigated the liquid surge and consequent contact with the condenser coil.) At each heat flux, steady-state conditions are considered to have been reached when the time-averaged variation of the wall superheat temperature, acquired every 3 seconds, is less than 0.0003 °C/s for 150 seconds. Under these conditions, time-averaged temperature data is obtained from 30 measurements collected over 90 seconds. The slope of the time-averaged thermocouple rake temperatures is used to calculate the heat flux, and to extrapolate the corresponding surface temperature. A detailed description of this data reduction method and uncertainty quantification are provided in [30]. The wall temperature and heat flux are near-uniform across the surface for all test cases, and the area-averaged uncertainties are approximately ±0.2 °C and ±4 kW/m^2 over the range of heat fluxes investigated.

3. Results and discussion

3.1. Nucleate boiling enhancement by free particles

Macroscopic images of boiling at a heat flux of 55 kW/m^2 from a single 13 mm non-spherical particle (Alfa Aesar) are shown in Fig. 2: the vapor bubbles generated are large enough to surround the entire millimeter-sized particle. While the particle oscillates on the heated surface during boiling due to the vapor bubble buoyant forces, it remains in contact with the heated surface and continually provides nucleation sites. Intense nucleate boiling is observed for the millimeter-sized free particle, in contrast to the polished surface. Fig. 3 shows a cycle of bubble ebullition from a narrow corner cavity formed between a single 13 mm spherical ball (Salem Specialty Ball Company) and the heated surface at the same heat flux of 55 kW/m^2. The visualization shows that a vapor bubble is generated at the narrow corner cavity, which then grows in size and departs from the surface. This vigorous vapor bubble generation caused by millimeter-sized free particles in water is the primary mechanism by which the heat transfer coefficient is enhanced compared to the polished surface. The remaining sections describe experimental investigation of the effect of particle size on boiling heat transfer performance using spherical copper particles; the trends and optimum particle size observed are supported with simplified models. Additional experimental inquiry on the effects of particle shape and number of particles (at constant particle size) are included in Appendix A.

3.2. Effect of the size of free particles

To identify the optimum free particle size for maximizing the boiling heat transfer performance in water, copper particles with sizes ranging from 20 nm to 13 mm were studied. The number of spherical millimeter-sized particles was chosen such that a single layer of particles covers the test surface (100, 25, 9, and 4 paticles for the 3, 6, 9, and 13 mm-diameter particles, respectively). For the sub-millimeter particles, a monolayer could not be ensured by counting; in this case, therefore, the mass of the particles placed on the surface was chosen so as to provide similar projected base coverage area as the four 13 mm particles assuming spherical particles and a tight packing density.

The experimental results for different free particle sizes are shown in the boiling curve in Fig. 4. As the size of the particles decreases from 13 mm to 3-6 mm, the overall boiling heat transfer performance improves (average surface superheats decrease for the same heat fluxes). However, as the particle size further decreases from 3 mm to 140-440 μm, the heat transfer performance decreases. Experiments using 10 μm and 20-40 nm particles (results not included in Fig. 4) were found to lead to even smaller improvements in heat transfer compared to the polished surface baseline, with virtually no enhancement being provided by 20-40 nm particles. The very small cavity sizes created by contact of these tiny

particles with the surface do not serve as active nucleation sites, and therefore cannot improve boiling heat transfer performance. For the free-particle technique, it is concluded that 3 mm to 6 mm particles are optimum when water is used as the working fluid. This suggests a different primary enhancement mechanism from previous studies in the literature which consider nanofluids [26,29,42] or fixed structures with sub-millimeter feature sizes [3,15,19,43-47] for pool boiling enhancement. The detailed trends in the boiling curves are discussed next for varying particle size; this is followed by a model-based validation of the postulated enhancement mechanism in section 3.3.

At low heat fluxes (< 50 kW/m^2), the relative performance of the particles of different sizes is dependent on boiling incipience and the number of activate nucleation sites. As the particle size decreases from 13 mm to 3 mm, the wall superheat at incipience decreases monotonically from 7.5°C to 2.5°C. The 3 mm particles show the best average heat transfer performance up to a heat flux of 50 kW/m^2. The performance deteriorates for a further decrease in particle size to 149-400 μm. The presence of an optimum particle size may be explained using vapor bubble nucleation theory. For spherical particles and constant fluid properties, a larger cavity size (*i.e.*, larger particle diameter) requires less superheat for nucleation incipience and bubble growth when considering only the shape of the narrow corner cavity [31]. However, since the particle itself impedes bubble departure under buoyant forces, large particles require bubbles to grow to a relatively larger size before their release. This tradeoff leads to an optimum particle size for minimum surface superheat at boiling incipience.

At higher heat fluxes, the optimum particle size shifts to a higher value. The slope of the boiling curve is sharper for the 6, 9, and 13 mm particles than it is for the 3 mm particles, resulting in a performance crossover at 50 kW/m^2, above which the 6 mm particles provide the best performance. Fig. 5 (a), (b) and (c) respectively show water boiling from a heated surface with one-hundred 3 mm particles, twenty-five 6 mm particles, and nine 9 mm particles at a heat flux of ~75 kW/m^2. Fig. 5 (d), (e), and (f) show corresponding macroscopic images of the same respective cases. It is clear from the images that the size of the vapor bubbles generated increases with increasing particle size at a constant heat flux, but the nucleation site density decreases. While the combination of mechanisms resulting in an optimum free particle size during vigorous boiling at high fluxes is less clear than at incipience, the current experimental results indicate that such a tradeoff exists. Under conditions of this experiment, the 6 mm particles provide the best thermal performance in terms of the total volume of vapor released from the surface at high heat fluxes, which is determined by a combination of the number of nucleation sites, bubble departure frequency, and the size of each vapor bubble.

3.3. Optimum particle size analysis

In section 3.2, the optimum particle size identified to provide the lowest surface superheat over the entire heat flux range investigated was shown to also yield the lowest wall superheat at incipience. The required boiling incipience superheat depends on the size of the free particles, which influences the surrounding liquid temperature profile and the vapor bubble growth, resulting in a tradeoff that leads to an optimum in free particle size. In order to explore this tradeoff for the range of particle sizes tested, the liquid temperature field adjacent to the heated surface is numerically simulated, while a force balance is used to predict vapor bubble growth and departure.

3.3.1. Force balance on vapor embryo

An analytical model is developed to predict the vapor bubble size required for departure from the surface. A vapor bubble embryo is assumed to originate from a narrow corner cavity between the flat surface and the spherical particle. Since bubbles are generated almost all around the circumference of the particle base, a two-dimensional axisymmetric representation of the particle, vapor, and liquid domains is used. The buoyant force, F_b, of the vapor bubble is calculated by estimating the shape and the size of the vapor bubble during growth. The resulting buoyant force is then compared to the surface tension-driven capillary force, F_c, in order to predict the required size of the bubble for release from the cavity. A similar model for predicting the bubble height required for detachment was developed by Wang *et al.* [48]. The model details and solution procedure for finding the bubble size at detachment are included in Appendix B.

The model shows that the bubble size required for detachment depends only on the diameter of the particle. The calculated minimum heights of the vapor bubble at departure, $h_{b,dep}$, are 3.4, 3.1, 2.9, and 3.4 mm for the 3, 6, 9, and 13 mm diameter particles, respectively. This value of approximately 3 mm for the detachment height in water compares favorably with other studies in the literature. Jones *et al.* [3] showed that the vapor bubble height at nucleation incipience from roughened surfaces was ~3.5 mm in water, and Wang *et al.* [48] predicted a departure height of 4.7 mm from a bed of packed glass spheres. The force balance model results are also in good agreement with the qualitative experimental observations in the current study (Fig. 5). It is noted that the model used here is applicable for relatively large particle sizes; with the more complex solid-liquid-vapor interactions that may be expected in layers of sub-microscale particles or with a mixture of different-sized particles, the underlying force balance assumptions for buoyancy and capillary forces used here would be altered.

3.3.2. Near-wall liquid superheat thermal model

While the force balance model referenced above predicts the required bubble height at departure, Hsu's theory [35,36] requires the temperature of the liquid surrounding a bubble to be superheated to enable growth. Thus, in order for the vapor bubble to grow to the required height for detachment, $h_{b,dep}$,

the surrounding liquid up to this height should be superheated. Three-dimensional numerical simulations are performed to compute the liquid temperature profile as a function of the surface heat flux for cases of a 3 mm- and a 9 mm-diameter particle. The heat flux (and associated surface superheat) required to satisfy the superheated liquid region criterion is estimated by means of this approach.

A one-quarter symmetric domain including a single copper particle, the surrounding liquid, and the bottom heated surface are modeled. The mesh for this domain is generated using GAMBIT, and the commercial software package FLUENT [49] is used to solve diffusion in the solid domain and natural convection in the liquid domain under the prescribed boundary conditions shown in Fig. 6. The experimentally obtained heat flux is used as the bottom surface boundary condition. A constant temperature boundary condition is applied at the top of the liquid pool far from the heated surface. This constant temperature boundary condition is iterated until the numerical solution for fluid temperature at the height of the pool thermocouple matches the experimental measurement within ±0.3°C. The mesh resolution was increased until the numerical simulation results were observed to be independent of mesh size; this was achieved with a total of ~470,000 elements. The liquid temperature obtained at the height of the pool thermocouple changes by less than 0.03 °C if a model with 1,500,000 elements is used. The point contact between the free particle and the heated surface or an adjacent free particle is treated as resulting in a surface contact area that is 5% of the projected area of the sphere. The resulting liquid temperature contours are used to determine if the liquid is superheated around the bubble at the size required for departure for the given heat flux.

Results from the numerical simulations presented in Fig. 6 (b) and (c) show the liquid and solid temperatures along a diagonal plane in the one-quarter symmetry solution domain for a 3 mm and a 9 mm particle, respectively. The required height of the bubble for departure calculated from the force balance model is shown superposed on the temperature contour plots. The 3 mm particle causes an increase in temperature of the working fluid in the region where liquid must be superheated for vapor bubble detachment at the heat flux 19.5 kW/m^2 considered in Fig. 4. Conversely, at a comparable heat flux of 23.5 kW/m^2, the 9 mm particle protrudes further into the cooler liquid region, and conducts heat further away from the surface, rather than localizing heating to the liquid region as would be critical for vapor bubble superheating and detachment. Therefore, in the case of this larger particle size, the portion of the region where liquid should be superheated for bubble detachment is found to be below the saturation temperature at this heat flux. Due to insufficient liquid heating for the larger 9 mm particle, boiling incipience would be expected to first occur for the 3 mm particle at the bubble departure heights calculated by the force balance; this agrees with the experimental observations. The numerical results also explain the larger optimal free particle size for water (3 mm to 6 mm) compared to FC-72 (tens of

microns) considered in a companion study [30]. The lowered surface tension of FC-72 allows vapor departure at much smaller vapor bubble sizes, and the conductive particle should be much smaller in that case to effectively localize heating to the narrow corner cavity region.

3.4. Mixture of free particle sizes

The vapor embryo force balance and thermal models identify the advantage of larger particles for reducing the required vapor bubble departure size and of smaller particles for localized superheating of liquid near the substrate. To exploit this tradeoff, mixtures of different sizes of particles are tested. Of the several heuristically selected combinations of particles tested, a mixture of fifty 3 mm particles and fifteen 6 mm particles is found to provide the largest improvement to boiling heat transfer. The boiling curve for this case is included in Fig. 4. The particle mixture provides the same optimum performance as the one-hundred 3 mm particles at heat fluxes below 50 kW/m^2, and the twenty-five 6 mm particles at heat fluxes above 50 kW/m^2, effectively capitalizing on the best performance of each particle size. Fig. 7 shows images for the cases of the 3 mm particles alone compared to the mixture of 3 and 6 mm particles just following boiling incipience at respective surface superheats of 2.5°C and 2.8°C. The bubble departure size with the 3 mm particles is on the order of 3 mm, as shown in Fig. 7 (c); however, for the case of the mixture of 3 and 6 mm particles, the vapor bubbles at ONB are observed to be bigger than those in Fig. 7 (a). The proximity of smaller 3 mm particles, which effectively superheat the liquid for bubble growth, may increase the liquid temperature in the corner cavities of the 6 mm particles and help the larger particles generate vapor bubbles, thus improving boiling performance.

3.5. Heat transfer coefficient comparison

Boiling heat transfer enhancement is demonstrated by comparing the heat transfer coefficients in the presence of free particles to those with the polished surface without free particles at the same heat flux. Fig. 8 shows the heat transfer coefficients for several of the experiments as a function of heat flux. A single boiling enhancement metric may be obtained by averaging the percentage improvement over the entire heat flux range for which the experiments fall in the nucleate boiling regime (~20-100 kW/cm^2 for 3 mm and 6 mm free particles). The average percentage enhancement in nucleate boiling heat transfer coefficient for *n* data points in the heat flux range selected is quantified using

$$\frac{\sum_{i=1}^{n} \frac{\left(h_i - h_{p,i}\right)}{h_{p,i}} \times 100 \times \left(q_i'' - q_{i-1}''\right)}{q_n'' - q_{i-1}''} \tag{10}$$

where h and h_p are the heat transfer coefficients of the experimental case and the polished surface baseline case at each heat flux. Using this definition, the nucleate boiling heat transfer enhancement achieved by the addition of millimeter-sized spherical free particles is presented in Table 1. The boiling heat transfer is seen to improve by as much as 115% compared to the case of a polished surface when an optimum mixture of 3 mm and 6 mm particles are used.

Conclusions

A free-particles-based boiling enhancement technique is studied using water as the working fluid. Free metal particles placed on a heated surface are found to improve boiling heat transfer by providing active nucleation sites, with the enhancement being a function of the number and size of the particles introduced. An experimentally observed optimum particle size of 3 mm to 6 mm, depending on the heat flux, was identified. Of the uniform particle size test cases, the largest average heat transfer coefficient over the range of heat fluxes tested was provided by the 3 mm particles with the lowest incipience wall superheat at the onset of nucleate boiling. Models developed for vapor bubble embryo growth and incipience corroborate that the lowest incipience superheat is required at these experimentally observed optimum particles sizes. In order to maximize the boiling heat transfer performance, and exploit the mechanistic tradeoff between a large particle size for ease of bubble growth/departure and a small particle size for more effective superheating of the surrounding liquid, mixtures of different sizes of particles were tested. A mixture of 3 mm and 6 mm particles was shown to improve the average heat transfer coefficient by 115% compared to a polished surface over a heat flux range from 20 to 100 kW/m^2.

Acknowledgements

Funding for this work from the Cooling Technologies Research Center, an NSF IUCRC at Purdue University, is gratefully acknowledged. Significant assistance was provided by Dr. Justin Weibel in the preparation of this manuscript.

Appendix A. Effects of the number and shape of free particles

Effects of the number and shape of particles on the boiling heat transfer enhancement with free particles explored in this work are investigated here using a set of copper particles that are not truly spherical in shape. The sphericity Ψ ($\pi^{1/3}(6V)^{2/3}A_s^{-1}$) was found to be approximately 0.9 based on estimates of the total surface area and volume of individual particles.

In order to investigate the effect of the number of free particles on boiling heat transfer, an increasing number of particles were placed in successive tests on the polished copper surface. The heat source area

accommodates up to four 13 mm-diameter particles in a single layer. Fig. A1 shows the boiling curves for each test case. The trends in the individual boiling curves for the different particle numbers are discussed below.

Independent of the number of free particles, heat transfer to the fluid first occurs by natural convection until the onset of nucleate boiling (ONB) occurs after a surface temperature overshoot, as shown in Fig. A1. The overshoot was more noticeable in the transient temperature data (not shown) than is revealed by the steady-state points on the boiling curve. The sharp reduction in wall superheat indicates a significant enhancement in the heat transfer coefficient due to transition from natural convection to boiling. Each particle on the heated surface has the potential to seed such large vapor bubbles, with each activation being associated with a temperature overshoot in the boiling curve. Nucleation site activation occurs at a unique superheat temperature for each specific non-spherical particle due to small variations in the cavity geometry formed with the surface. Therefore, multiple incipience events occur over a range of heat fluxes for the surfaces with free particles, compared to the polished surface for which bubble nucleation incipience is a single event a heat flux of ~40 kW/m^2.

Unlike the experiments with two or more free particles of 13 mm diameter, for which the position of a particle is confined by the side walls and other particles, particle motion is relatively unrestricted for the case of a single copper particle. Thus, when boiling begins, the particle is pushed by vapor release from the narrow corner cavity and moves on the surface through a translational or rolling motion. If a cavity geometry formed between the particle and the surface is not conducive to bubble nucleation, boiling is suppressed. The sharp increase in wall superheat that results again renders the site active for nucleation. This causes multiple incipience overshoot events even for a single particle, as observed in Fig. A1. At higher heat fluxes, the particle continually provides active nucleation sites regardless of the nature of contact due to the large surface superheat.

The experiments with four 13 mm particles are used to describe the boiling curve trends following initial incipience when multiple particles are placed on the surface. Fig. A2 shows macroscopic visualizations of the nucleate boiling heat transfer phenomena with increasing heat flux for this case. In the low heat flux range, below 37 kW/m^2, heat transfer occurs by natural convection. When the heat flux reaches 37 kW/m^2, nucleate boiling is initiated and vapor bubbles depart from the narrow corner cavities. In this case, incipience occurs simultaneously at the two rear particles in the image in Fig. A2 (a). Due to the efficient thermal energy transfer from the heated surface by means of the large vapor bubbles generated, the wall superheat immediately decreases by approximately 1°C at incipience as shown in the inset of Fig. A1. At a heat flux of 45 kW/m^2, a nucleation site activates at the base of the particle placed at the left front corner in the image in Fig. A2 (b). As the heat flux is further increased and reaches 72

kW/m^2, boiling is initiated at the last of the four particles. Each time an individual particle provides a new nucleation site, a small corresponding decrease in the wall superheat is observed in Fig. A2.

This succession of incipience events, and the associated reductions in wall superheat, explain the trend in wall superheat at 100 kW/m^2 for the increasing number of particles shown in Table A1. At this heat flux, all individual particles for each test case are actively supporting boiling. As shown in Table 1, the boiling regime wall superheat decreases with an increasing number of free particles. The surface with four particles maintains comparatively low wall superheats due to an increased number of nucleation sites at high heat fluxes. For the surfaces with fewer particles, much of the heated polished surface area remains in the convection heat transfer regime even at 100 kW/m^2, which is the reason for the lower overall surface heat transfer coefficient.

A brief discussion of the effect of particle shape on boiling performance is warranted based on the differing results between non-spherical (Fig. A1) and spherical (Fig. 4) 13 mm particles. The four non-spherical particles considered in Fig. A1 maintain the wall superheat at approximately 7 °C for the highest heat flux investigated, whereas the four 13 mm spherical free particles presented in Fig. 4 reach a maximum surface superheat of over 10 °C. Therefore, the shape of the free particles clearly has a significant influence on boiling heat transfer. The shape of the free particles placed on a heated surface affects various boiling parameters such as the contact area between the particles and the heated surface, the shape and the angle of narrow corner cavities, and mixing of the fluid trapped in the cavities. Further study on the effect of the free particle shape is required to fully understand these trends.

Appendix B. Force balance model solution procedure

An analytical model is developed to predict the vapor bubble size required for departure from the surface, as depicted in Fig. A3 (a). The solution procedure used to find the size of a bubble at detachment is as follows:

1. Assume an initial small value of x_c, the x-location of the liquid-vapor-particle contact point.
2. For the given x_c, calculate the geometry and size of the vapor bubble.
3. Obtain the centroid of the vapor bubble.
4. Calculate the particle contact point of force and the directional line of force (surface tangent at the point of force).
5. Find the magnitude and direction of the buoyant force, F_b, and capillary forces, F_{ct} and F_{cb}.
6. Project the buoyant and capillary forces onto the line of force and compare the effective buoyant force, F_{eb}, against the effective capillary force, F_{ec}.

7. Iterate steps 1 through 6 until the effective buoyant force equals the effective capillary force as x_c is incrementally increased; this vapor bubble size is assumed to be the minimum required for departure.

The shape of the vapor bubble is defined by the equilibrium contact angle, θ, and is assumed to be 40 deg based on the contact angle observed in Fig. 3. The size of the bubble, A_b, is decomposed into two parts as shown in Fig. A3 (b). Using the assumptions of $w = x_b$ and $\alpha = (\alpha_1+\alpha_2)/2$ to simplify the model (based on visual observations of bubble growth for the current geometry and working fluid), the decomposed areas can be calculated as

$$A_1 = \frac{1}{2}\left(x_c h - R^2\left(\theta_c - \sin\theta_c\right)\right) \tag{A1}$$

$$A_2 = \int_{x_c}^{x_b}\left[\sqrt{r_b^2 - \left(x - x_{cc}\right)^2} + r_p - y_{cc}\right]dx + \int_{x_b}^{x_{cc}+r_b}\left[2\sqrt{r_b^2 - \left(x - x_{cc}\right)^2}\right]dx, \text{ when } y_c > 0 \tag{A2}$$

$$= \int_{x_c}^{r_p}\left[\sqrt{r_b^2 - \left(x - x_{cc}\right)^2} + r_p - y_{cc} - 2\sqrt{r_p^2 - x^2}\right]dx + \int_{r_p}^{x_b}\left[r_p - y_{cc} + \sqrt{r_b^2 - \left(x - x_{cc}\right)^2}\right]dx$$

$$+ \int_{x_b}^{x_{cc}+r_b}\left[2\sqrt{r_b^2 - \left(x - x_{cc}\right)^2}\right]dx, \text{ when } y_c < 0$$

where r_b and (x_{cc}, y_{cc}) are the radius and the coordinate of the center of the concave part of A_2, respectively, which are

$$r_b = \frac{m}{2\cos\left(\left|\pi/2 - \alpha\right|\right)} \tag{A3}$$

$$x_{cc} = x_b - r_b \cdot \cos\left(\operatorname{atan}\left(\frac{h}{x_b - x_{cb}}\right) + \alpha - \frac{\pi}{2}\right) \tag{A4}$$

$$y_{cc} = R - r_b \cdot \sin\left(\operatorname{atan}\left(\frac{h}{x_b - x_{cb}}\right) + \alpha - \frac{\pi}{2}\right) \tag{A5}$$

The centroid of the bubble is obtained by finding the point of intersection point between two lines that divide the area of the bubble in half, which are $y_1(x)$ and the vertical line $x = c$ as defined in Fig. A3 (c). The vertical line $x = c$, in which c is a constant, is found by integrating the area of the bubble from (0, r_p) along the x-axis until the integrated area becomes half of the total bubble volume.

The point of force is the location where a vertical extension from the centroid meets the surface of the spherical particle. The line of force is the surface tangent at the point of force. The magnitudes of the buoyant force which acts to pull the bubble from the cavity, and the capillary forces which hold the bubble to the surface, can be expressed as

$$F_b = \rho_w A_b (-g) \tag{A6}$$

$$F_{ct} = F_{cb} = \sigma_w \tag{A7}$$

assuming the water vapor density is negligible compared to the liquid density.

The magnitudes of each force are projected on the line of force and converted into effective values as shown in Fig. A3 (d). The two components of the capillary force that are projected onto the line of force sum as the total effective capillary force, F_{ec}. In order for the bubble to be released from the cavity, the effective buoyant force should be larger than the effective capillary force. If this criterion is not satisfied, the size of the bubble is iteratively increased by moving the contact point along the surface of the particle further from the base. The procedure continues until the effective buoyant force just exceeds the effective capillary force, which is regarded as the minimum size of the bubble for detachment.

References

[1] R. L. Webb, The evolution of enhanced surface geometries for nucleate boiling, Heat Transfer Engineering, 2 (3–4) (1981) 46–69.

[2] H. M. Kurihari, J. E. Myers, Effects of superheat and roughness on the boiling coefficients, AlChE Journal 6 (1960) 83–91.

[3] B. J. Jones, J. P. McHale, S. V. Garimella, The influence of surface roughness on nucleate pool boiling heat transfer, Journal of Heat Transfer 131 (12) (2009) 121009.

[4] S. T. Hsu, F. W. Schmidt, Measured variations in local surface temperatures in pool boiling of water, Journal of Heat Transfer 83 (1961) 254–260.

[5] P. J. Marto, W. M. Rohsenow, Effects of surface conditions on nucleate pool boiling of sodium, Journal of Heat Transfer 88 (1966) 196–203.

[6] M. Jakob, Heat Transfer, John Wiley & Sons, New York, 1949.

[7] C. Corty, A. S. Foust, Surface variables in nucleate boiling, Chemical Engineering Progress Symposium Series 17 (1955) 1–12.

[8] I. H. Chaudhri and I. R. McDougall, Ageing studies in nucleate pool boiling of isopropyl acetate and perchloroethylene, International Journal of Heat and Mass Transfer 12 (6) (1969) 681–688.

[9] R. I. Vachon, G. H. Nix, G. E. Tanger, and R. O. Cobb, Pool boiling heat transfer from teflon-coated stainless steel, Journal of Heat Transfer 91 (3) (1969) 364–369.

[10] R. K. Young, R. L. Hummel, Improved nucleate boiling heat transfer, Chemical Engineering Progress Symposium Series 61 (1965) 264–267.

[11] P. Griffith, J. D. Wallis, The role of surface conditions in nucleate boiling, Chemical Engineering Progress Symposium Series 56 (1960) 49–63.

[12] A. R. Betz, J. Jenkins, C.-J. Kim, and D. Attinger, Boiling heat transfer on superhydrophilic, superhydrophobic, and superbiphilic surfaces, International Journal of Heat and Mass Transfer 57 (2) (2013) 733–741.

[13] S. G. Liter, M. Kaviany, Pool-boiling CHF enhancement by modulated porous-layer coating: theory and experiment, International Journal of Heat and Mass Transfer 44 (2001) 4287–4311.

[14] R. M. Milton, U.S. Pat. 3384154, 1968.

[15] A. E. Bergles, M. C. Chyu, Characteristics of nucleate pool boiling from porous metallic coatings, Journal of Heat Transfer 104 (1982) 279–285.

[16] V. I. Borzenko, S. P. Malyshenko, Mechanisms of phase exchange under conditions of boiling on surfaces with porous coatings, High Temperature 39 (5) (2001) 714–721.

[17] W. Nakayama, T. Daikoku, H. Kuwahara, T. Nakajima, Dynamic model of enhanced boiling heat transfer on porous surface - Part I: Experimental investigation, Journal of Heat Transfer 102 (1980) 451–456.

[18] M. S. El-Genk, J. L. Parker, Enhanced boiling of HFE-7100 dielectric liquid on porous graphite, Energy Conversion and Management 46 (2005) 2455–2481.

[19] C. Li, G. P. Peterson, Parametric study of pool boiling on horizontal highly conductive microporous coated surfaces, Journal of Heat Transfer 129 (11) (2007) 1465–1475.

[20] J. J. Wei, H. Honda, Effects of fin geometry on boiling heat transfer from silicon chips with micro-pin-fins immersed in FC-72, International Journal of Heat and Mass Transfer 46 (21) (2003) 4059–4070.

[21] K. N. Rainey, S. M. You, Pool boiling heat transfer from plain and microporous, square pin-finned surfaces in saturated FC-72, Journal of Heat Transfer 122 (2000) 509–516.

[22] S. M. You, T. W. Simon, A. Bar-Cohen, A technique for enhancing boiling heat transfer with application to cooling of electronic equipment, IEEE Transactions on Components, Hybrids and Manufacturing Technology 15 (5) (1992) 823–831.

[23] J. P. O'Connor, S. M. You, A painting technique to enhance pool boiling heat transfer in saturated FC-72, Journal of Heat Transfer 117 (1995) 387–393.

[24] K. J. Park, D. Jung, Enhancement of nucleate boiling heat transfer using carbon nanotubes, International Journal of Heat and Mass Transfer 50 (2007) 4499–4502.

[25] D. Wen, Y. Ding, Experimental investigation into the pool boiling heat transfer of aqueous based γ-alumina nanofluids, Journal of Nanoparticle Research 7 (2005) 265–274.

[26] S. B. White, A. J. Shih, and K. P. Pipe, Effects of nanoparticle layering on nanofluid and base fluid pool boiling heat transfer from a horizontal surface under atmospheric pressure, Journal of Applied Physics 107 (11) (2010) 114302.

[27] P. Vassallo, R. Kumar, S. D'Amico, Pool boiling heat transfer experiments in silica–water nano-fluids, International Journal of Heat and Mass Transfer 47 (2004) 407–411.

[28] S. M. You, J. H. Kim, K. H. Kim, Effect of nanoparticles on critical heat flux of water in pool boiling heat transfer, Applied Physics Letters 83 (16) (2003) 3374–3376.

[29] S. J. Kim, I. C. Bang, J. Buongiorno, L. W. Hu, Surface wettability change during pool boiling of nanofluids and its effect on critical heat flux, International Journal of Heat and Mass Transfer 50 (2007) 4105–4116.

[30] T. Y. Kim, J. A. Weibel, S. V. Garimella, A free-particles-based technique for boiling heat transfer enhancement in a wetting liquid, International Journal of Heat and Mass Transfer, (in review).

[31] J. Li, P. Cheng, Bubble cavitation in a microchannel, International Journal of Heat and Mass Transfer 47 (2004) 2689–2698.

[32] Y.-Y. Hsu, On the size range of active nucleation cavities on a heating surface, Journal of Heat Transfer 84 (1962) 207–216.

[33] Y.-Y. Hsu, R.W. Graham, Transport Processes in Boiling and Two-Phase Systems, Hemisphere, Washington, DC, 1976.

[34] W. Wu, J.-H. Du, X.-J. Hu, B.-X. Wang, Pool boiling heat transfer and simplified one-dimensional model for prediction on coated porous surfaces with vapor channels, International Journal of Heat and Mass Transfer 45 (2002) 1117–1125.

[35] M. S. El-Genk, J. L. Parker, Nucleate boiling of FC-72 and HFE-7100 on porous graphite at different orientations and liquid subcooling, Energy Conversion and Management 49 (2008) 733–750.

[36] J. L. Parker, M. S. El-Genk, Effect of surface orientation on nucleate boiling of FC-72 on porous graphite, Journal of Heat Transfer 128 (2006) 1159–1175.

[37] L. H. Chai and D. S. Wen, Theoretical analyses on boiling critical heat flux with porous media, Heat Mass Transfer 41 (9) (2005) 780–784.

[38] V. K. Dhir, Boiling heat transfer, Annual Review of Fluid Mechanics 30 (1998) 365–401.

[39] D. Gorenflo, U. Chandra, S. Kotthoff, and A. Luke, Influence of thermophysical properties on pool boiling heat transfer of refrigerants, International Journal of Refrigeration 27 (5) (2004) 492–502.

[40] R. J. Benjamin and A. R. Balakrishnan, Nucleation site density in pool boiling of saturated pure liquids: Effect of surface microroughness and surface and liquid physical properties, Experimental Thermal and Fluid Science, 15 (1) (1997) 32–42.

[41] S. M. Sami and J. D. Comeau, Influence of thermophysical properties on two-phase flow convective boiling of refrigerant mixtures, Applied Thermal Engineering, 22 (14) (2002) 1535–1548.

[42] H. S. Xue, J. R. Fan, R. H. Hong, Y. C. Hu, Characteristic boiling curve of carbon nanotube nanofluid as determined by the transient calorimeter technique, Applied Physics Letters 90 (18) (2007) 184107.

[43] S. M. Kwark, M. Amaya, R. Kumar, G. Moreno, S. M. You, Effects of pressure, orientation, and heater size on pool boiling of water with nanocoated heaters, International Journal of Heat and Mass Transfer 53 (2010) 5199–5208.

[44] A. Pal and Y. Joshi, Boiling at sub-atmospheric conditions with enhanced structures, in: The Tenth Intersociety Conference on Thermal and Thermomechanical Phenomena in Electronics Systems (ITherm), San Diego, CA, pp. 620–629.

[45] J. P. McHale and S. V. Garimella, Bubble nucleation characteristics in pool boiling of a wetting liquid on smooth and rough surfaces, International Journal of Multiphase Flow 36 (4) (2010) 249–260.

[46] M. A. Hanlon and H. B. Ma, Evaporation heat transfer in sintered porous media, Journal of Heat Transfer 125 (4) (2003) 644–652.

[47] Z. Q. Chen, P. Cheng, and T. S. Zhao, An experimental study of two phase flow and boiling heat transfer in bi-dispersed porous channels, International Communications in Heat and Mass Transfer, 27 (3) (2000) 293–302.

[48] Z. Wang, X. F. Peng, and J. M. Ochterbeck, Dynamic bubble behavior during boiling in bead-packed structures, International Journal of Heat and Mass Transfer 47 (22) (2004) 4771–4783.

[49] Fluent Inc., FLUENT 6.2 User's Guide, Lebanon, NH, 2005.

Table 1. Boiling heat transfer enhancement versus the polished surface by addition of millimeter-sized spherical free particles in the heat flux range of 20 to 100 kW/m^2.

Particle size (number)	Nucleate boiling enhancement (%)
3 mm (50 EA) and 6 mm (15 EA)	115
3 mm (100 EA)	105
6 mm (25 EA)	99
9 mm (9 EA)	61
13 mm (4EA)	79

Table A2. Boiling heat transfer characteristics as a function of the number of free particles of 13 mm diameter.

Number of Particles	q'' at ONB (kW/m^2)	ΔT at 100 kW/m^2 (°C)
1	25.7	13.2
2	29.6	11.9
3	31.3	10.4
4	36.6	7.3

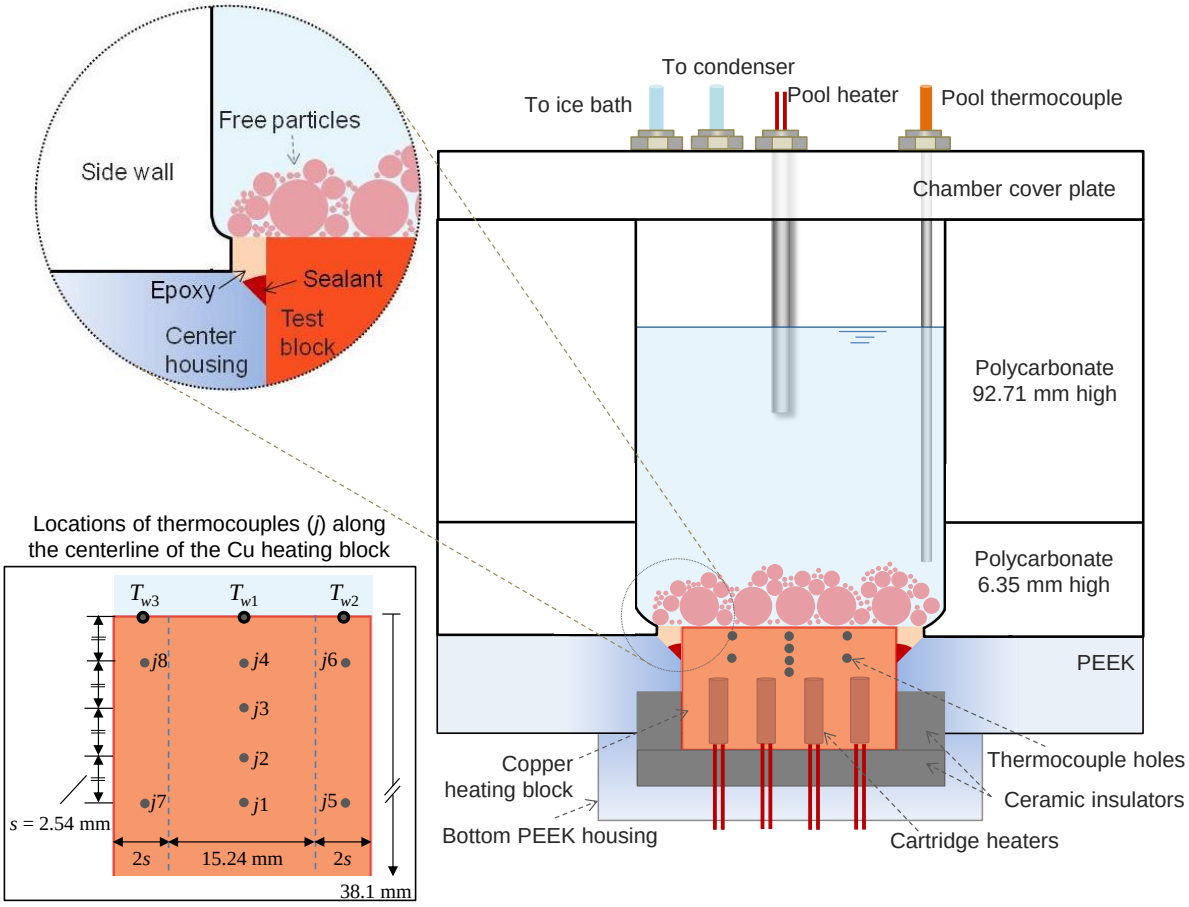

Fig. 1. Schematic diagram of the experimental setup.

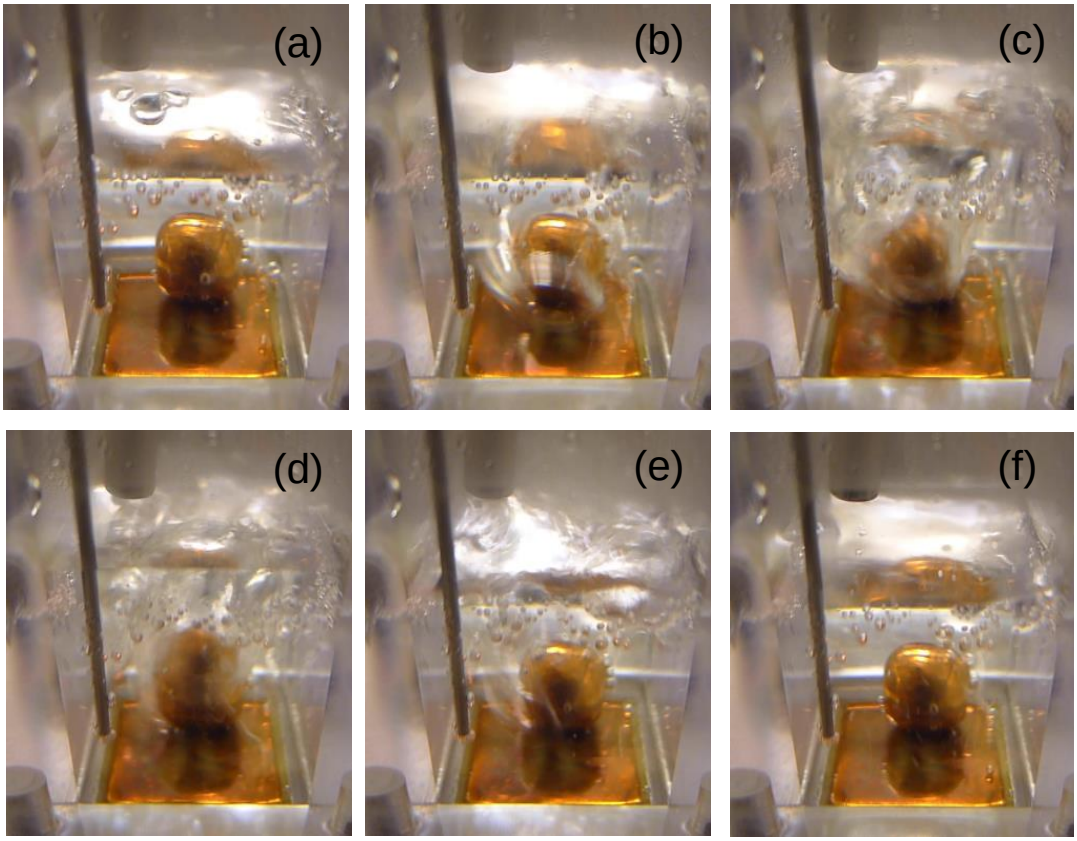

Fig. 2. Macroscale images of pool boiling from a single 13 mm copper particle at a heat flux of 55 kW/m^2. The images are extracted from a movie made available as Supplementary Data.

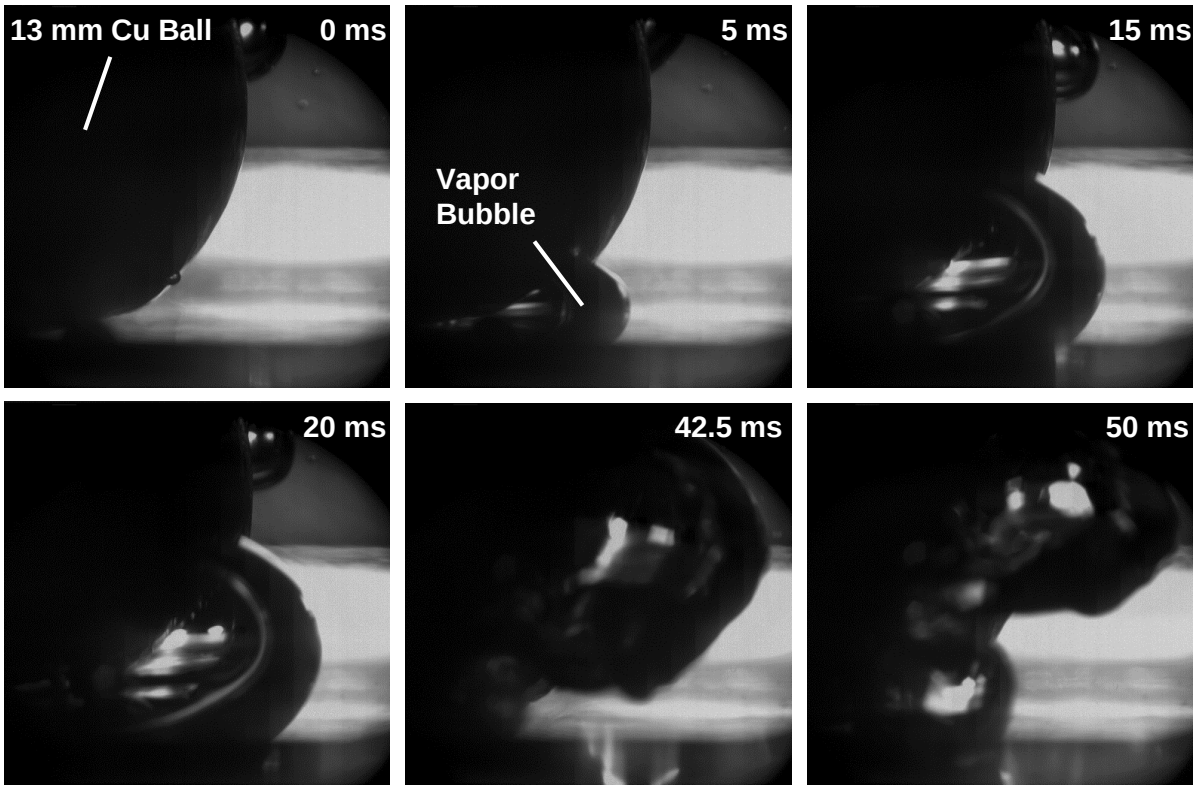

Fig. 3. A series of images showing nucleate boiling from the narrow corner cavity of a single 13 mm copper particle placed on a polished surface at 55 kW/m^2 in water. The images are extracted from high-speed video obtained at 4000 fps and made available as Supplementary Data.

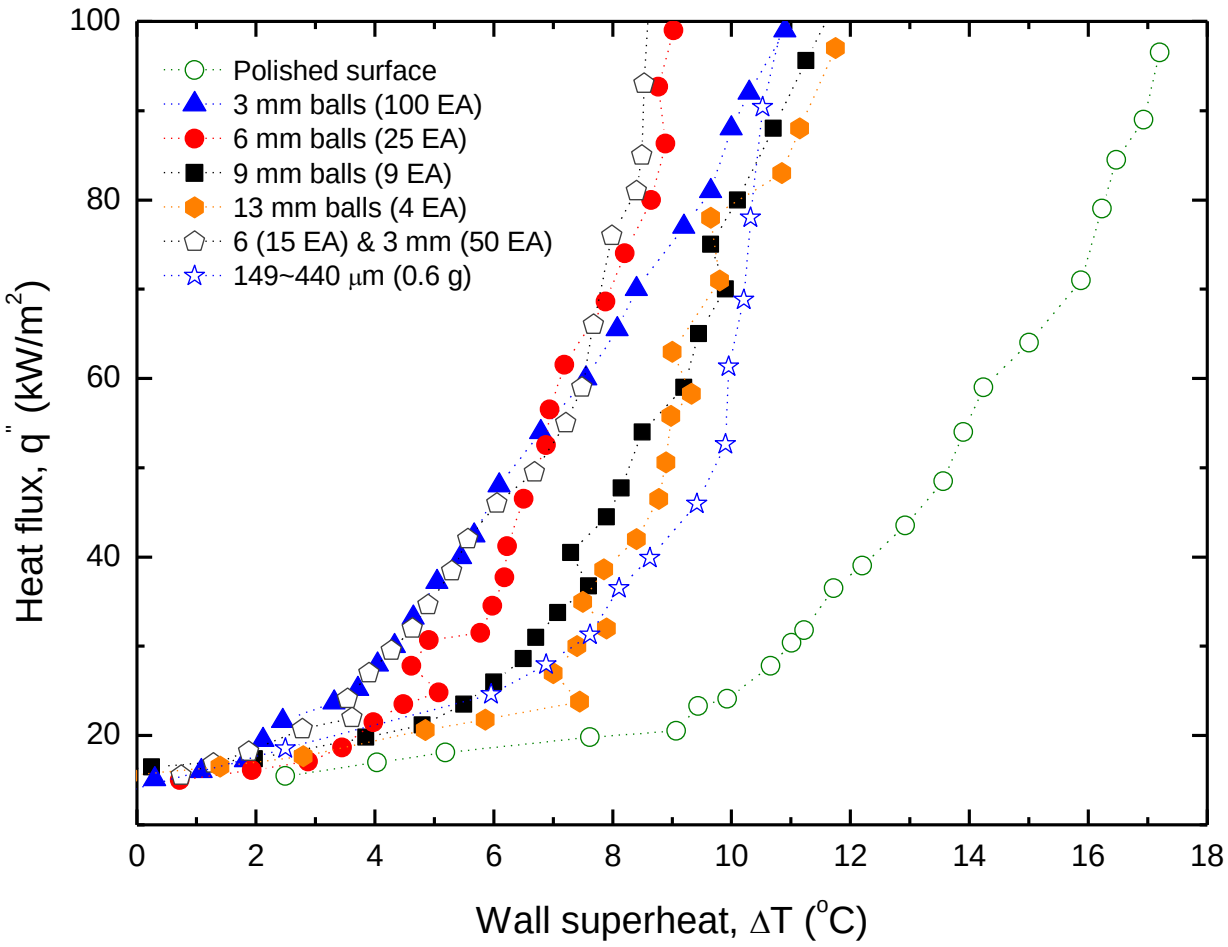

Fig. 4. Boiling curve showing the effect of the free particle size on boiling heat transfer. The experimental results for 10 μm and 20-40 nm particles are not shown.

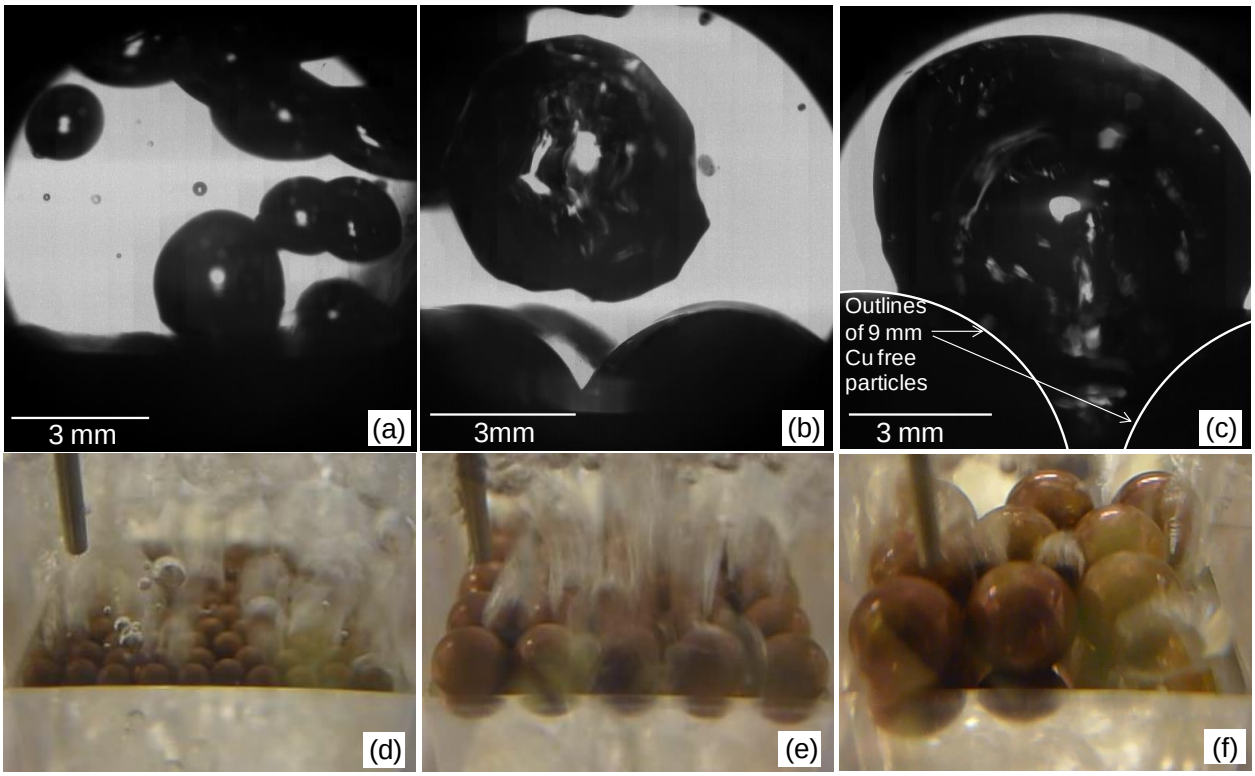

Fig. 5. High-speed microscopic visualization of the nucleate boiling characteristics for (a) one-hundred 3 mm particles at 77 kW/m^2, (b) twenty-five 6 mm particles at 74 kW/m^2, and (c) nine 9 mm particles at 75 kW/m^2. Macroscopic views for the same respective cases are shown in (d), (e), and (f).

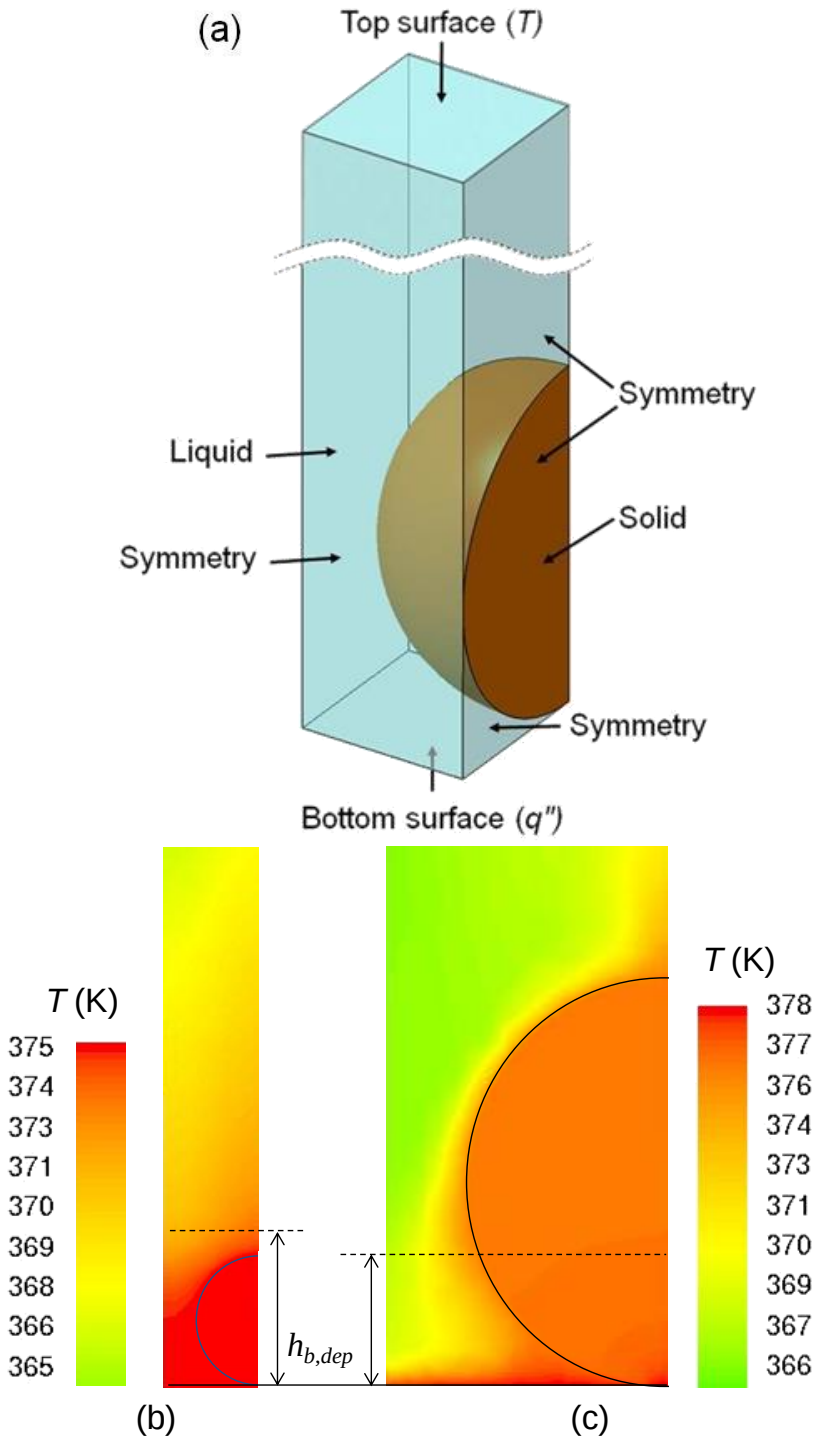

Fig. 6. Numerical simulation: (a) boundary conditions, and results that show the particle and liquid temperature profile for (b) a 3 mm-diameter free particle at the heat flux of 19.5 kW/m^2, and for (c) a 9 mm-diameter free particle at 23.5 kW/m^2. The height of a vapor bubble required for departure from the heated surface, $h_{b,dep}$, obtained from the buoyant versus capillary force balance is superposed.

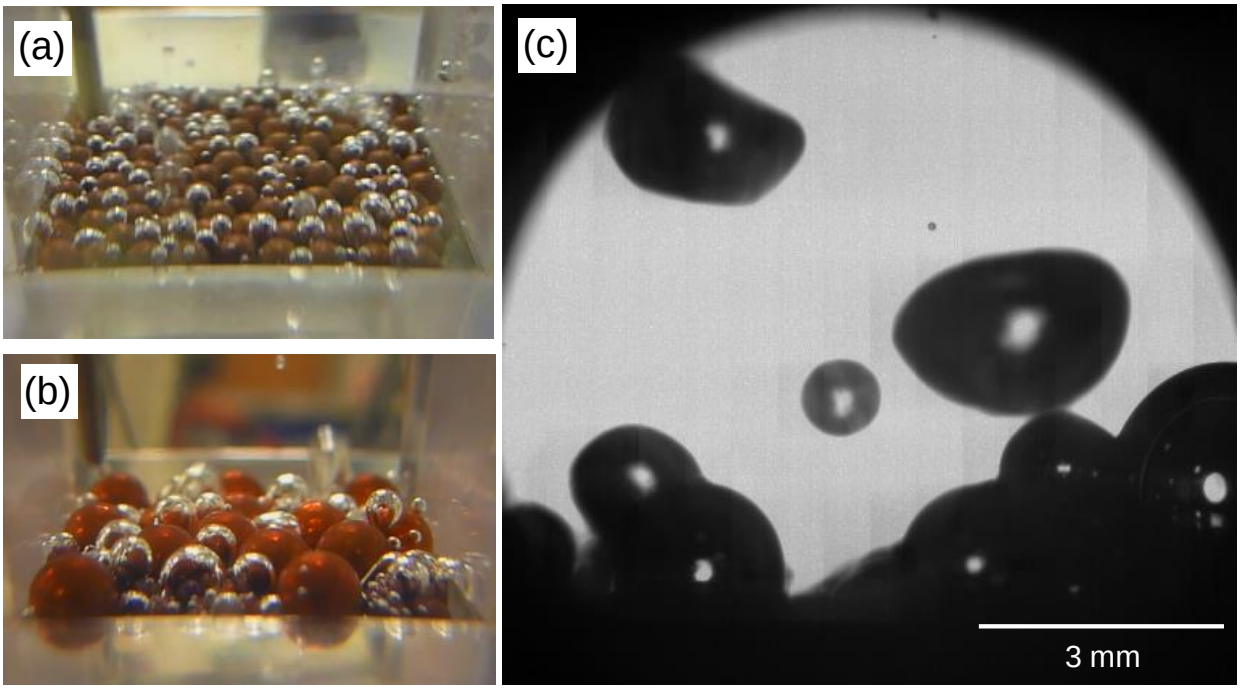

Fig. 7. A comparison of vapor bubble size at onset of nucleation boiling for (a) one-hundred 3 mm particles, (b) a mixture of fifty 3 mm particles and fifteen 6 mm particles, and (c) a microscopic view of case (a).

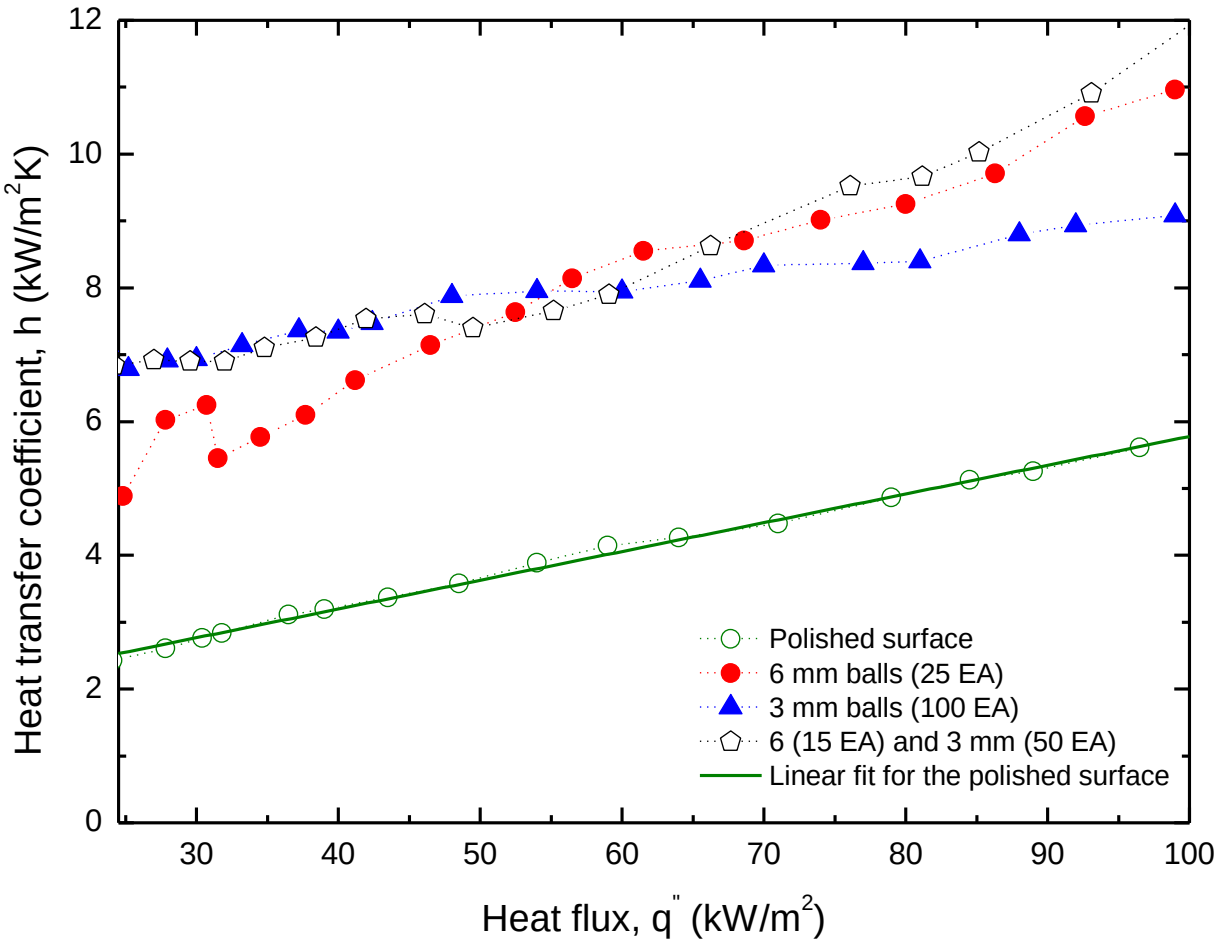

Fig. 8. Boiling heat transfer coefficients as a function of input heat flux for 3 mm and 6 mm free particles.

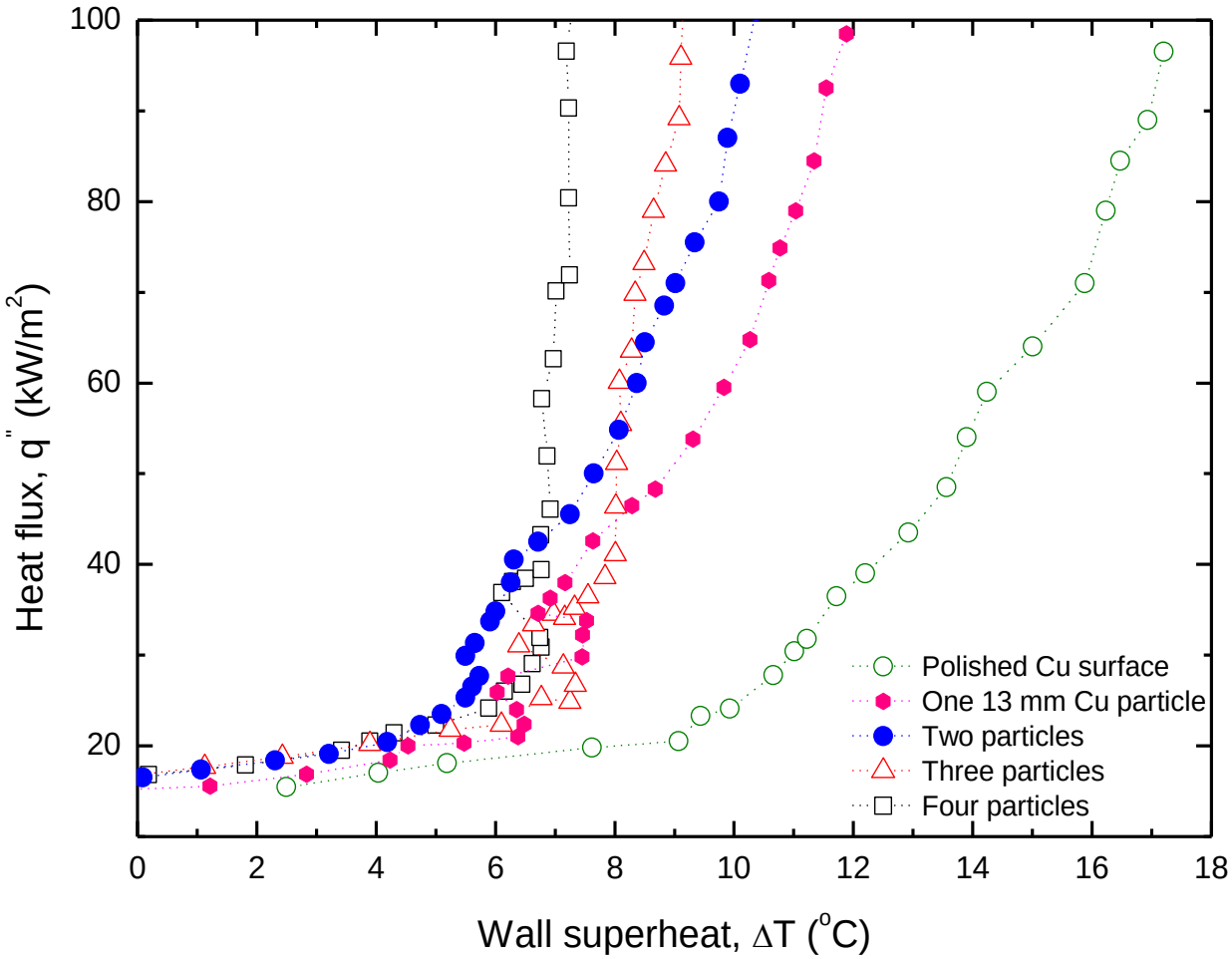

Fig. A1. Boiling curve showing the effect of number of 13 mm-diameter non-spherical free particles on boiling heat transfer.

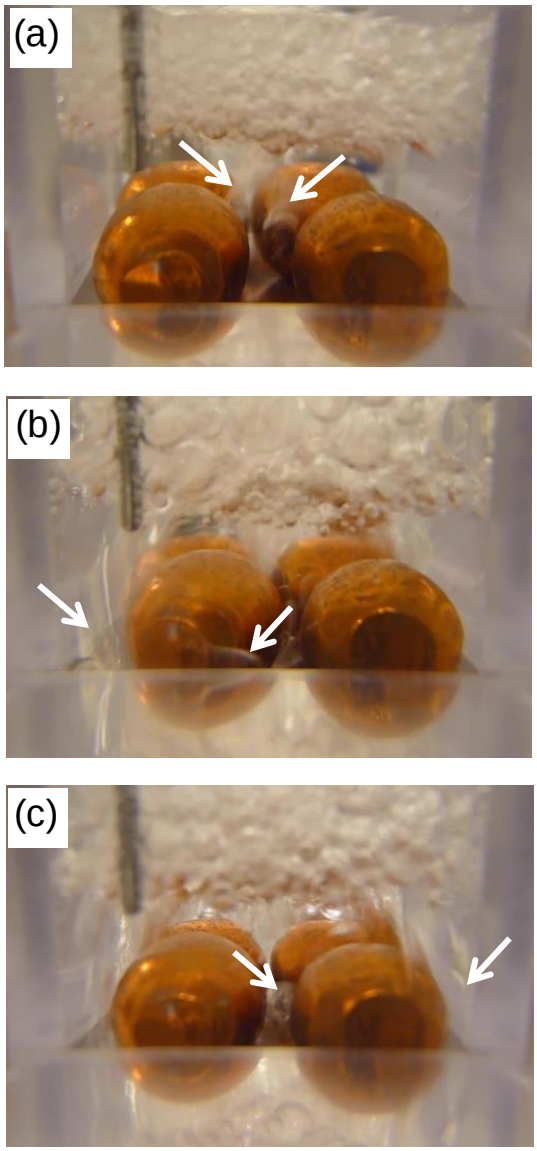

Fig. A2. Macroscopic visualization of nucleate boiling from four 13 mm non-spherical free copper particles at heat fluxes of (a) 37 kW/m^2, (b) 45 kW/m^2, and (c) 72 kW/m^2. Arrows in each image indicate the vapor bubbles generated by newly activated free particles at the corresponding heat flux.

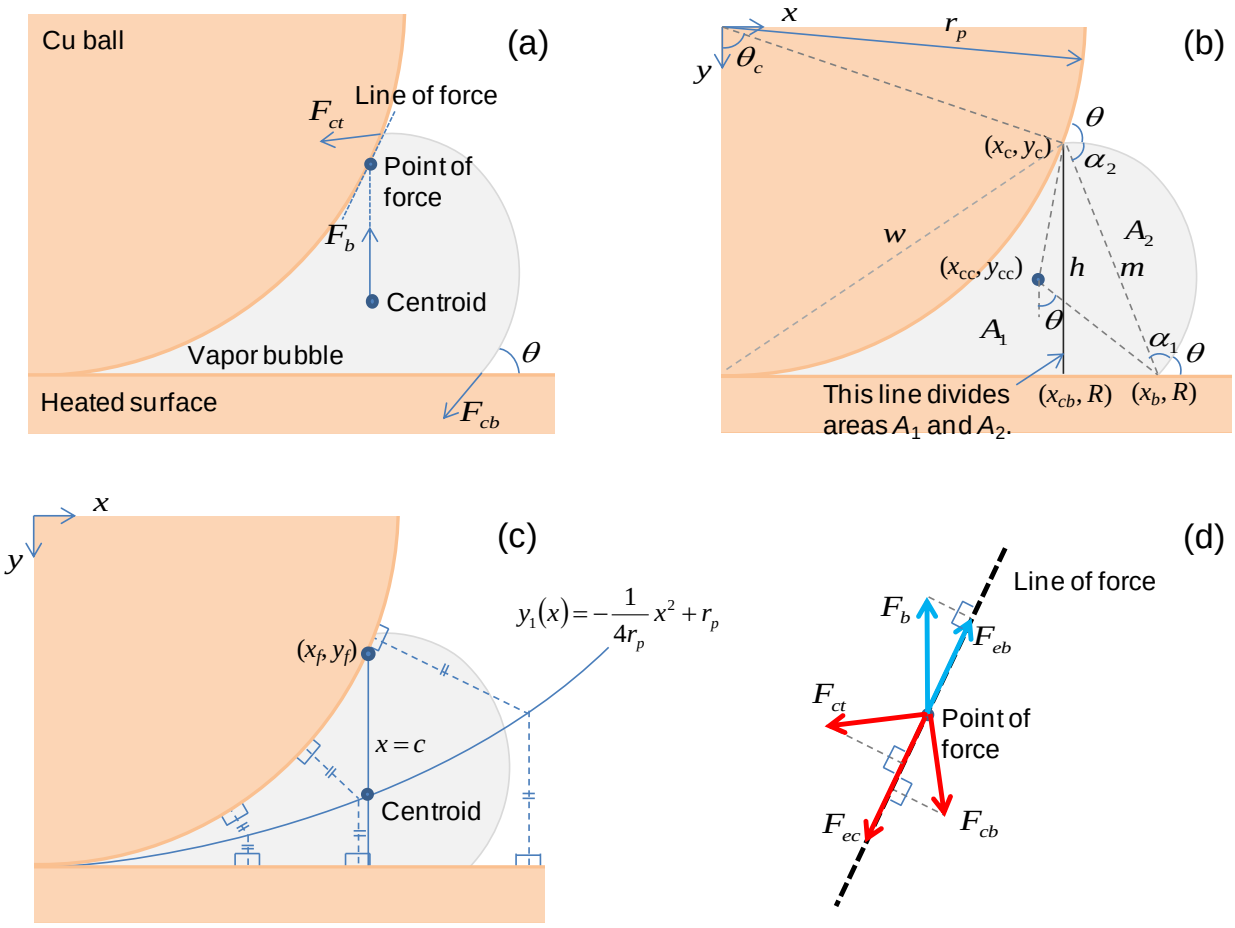

Fig. A3. Schematic diagram of the vapor embryo force balance model for a spherical particle on a heated surface. The model is used to determine the size of a vapor bubble required for release from the cavity. The diagram shows the (a) force balance diagram, (b) decomposed bubble geometry, (c) equation for centroid of the bubble, and (d) the effective buoyant force and capillary forces.